



AMERICAN METEOROLOGICAL SOCIETY

Journal of Climate

EARLY ONLINE RELEASE

This is a preliminary PDF of the author-produced manuscript that has been peer-reviewed and accepted for publication. Since it is being posted so soon after acceptance, it has not yet been copyedited, formatted, or processed by AMS Publications. This preliminary version of the manuscript may be downloaded, distributed, and cited, but please be aware that there will be visual differences and possibly some content differences between this version and the final published version.

The DOI for this manuscript is doi: 10.1175/JCLI-D-13-00246.1

The final published version of this manuscript will replace the preliminary version at the above DOI once it is available.

If you would like to cite this EOR in a separate work, please use the following full citation:

Barnes, E., N. Barnes, and L. Polvani, 2013: Delayed Southern Hemisphere climate change induced by stratospheric ozone recovery, as projected by the CMIP5 models. *J. Climate*. doi:10.1175/JCLI-D-13-00246.1, in press.



1 **Delayed Southern Hemisphere climate change induced by**
2 **stratospheric ozone recovery, as projected by the CMIP5 models**

3 ELIZABETH A. BARNES *

Lamont-Doherty Earth Observatory, Columbia University, Palisades, New York

NICHOLAS W. BARNES

Department of Computer Science and Engineering, University of Minnesota, Minneapolis, MN

AND LORENZO M. POLVANI

*Lamont-Doherty Earth Observatory and
the Department of Applied Physics and Applied Math of Columbia University, New York, NY*

submitted to J. Climate August 5, 2013

*Corresponding author address: Elizabeth A. Barnes, Department of Atmospheric Science, Colorado State University, 1371 Campus Delivery, Fort Collins, CO 80523-1371.

E-mail: eabarnes@atmos.colostate.edu

ABSTRACT

4
5 Stratospheric ozone is expected to recover by the end of this century due to the regulation
6 of ozone depleting substances by the Montreal Protocol. Targeted modeling studies have
7 suggested that the climate response to ozone recovery will greatly oppose the climate response
8 to rising greenhouse-gas (GHG) emissions. However, the extent of this cancellation remains
9 unclear since only a few such studies are available. Here, we analyze a much larger set
10 of simulations performed for the Coupled Model Intercomparison Project, phase 5, all of
11 which include ozone recovery. We show that the closing of the ozone hole will cause a
12 delay in summer-time (DJF) Southern Hemisphere climate change, between now and 2045.
13 Specifically, we find that the position of the jet stream, the width of the subtropical dry-zones,
14 the seasonality of surface temperatures, and sea ice concentrations all exhibit significantly
15 reduced summer-time trends over the first half of the 21st Century as a consequence of
16 ozone recovery. After 2045, forcing from GHG emissions begins to dominate the climate
17 response. Finally, comparing the relative influences of future GHG emissions and historic
18 ozone depletion, we find that the simulated DJF tropospheric circulation changes between
19 1965-2005 (driven primarily by ozone depletion) are larger than the projected changes in
20 any future scenario over the entire 21st Century.

21 1. Introduction

22 Polar stratospheric ozone depletion has induced changes in the Southern Hemisphere
23 climate with observational evidence of its impact on the atmospheric (Roscoe and Haigh
24 (2007); Lee and Feldstein (2013); see Thompson et al. (2011) for a recent review), oceanic
25 (Vaugh et al. 2013), and hydrological (Kang et al. 2011) circulations. Modeling-based
26 studies have documented the impact of the Montreal Protocol in mitigating future sea ice
27 loss (Smith et al. 2012) and changes in the earth’s hydroclimate (Wu et al. 2013) that would
28 have occurred with unabated stratospheric ozone depletion. Looking to the future, the effects
29 of stratospheric ozone recovery on Southern Hemisphere climate are expected to counter-act
30 the effects of greenhouse gas warming (e.g. Arblaster et al. (2011); Polvani et al. (2011a);
31 McLandress et al. (2011); Wilcox et al. (2012)).

32 Previous studies have focused on targeted, ozone-on, ozone-off simulations to determine
33 the importance of past and future stratospheric ozone changes on the climate system (e.g.
34 Sigmond and Fyfe (2010); Polvani et al. (2011b); Smith et al. (2012); Wu et al. (2013)).
35 While these single-forcing model experiments are clean and unambiguous tools to determine
36 the influence of ozone recovery on global climate, they inherently exclude feedbacks between
37 the transient greenhouse-gas induced response and the response due to ozone recovery. Ad-
38 ditional studies (e.g. McLandress et al. (2011); Polvani et al. (2011a)) analyze output from
39 a single coupled general circulation model that is forced with both greenhouse gases (GHG)
40 and stratospheric ozone depletion and recovery, and thus, are able to quantify the relative
41 importance of stratospheric ozone recovery on future climate trends.

42 The climate models run for the Coupled Model Intercomparison Projects (CMIP) offer

43 an important, additional data set to explore the role of ozone recovery over the coming
44 century in a large multi-model ensemble. As is now well documented (Cordero and Forster
45 2006; Son et al. 2008b), only a subset of the models run for the CMIP3 (CMIP phase 3)
46 included time-varying stratospheric ozone (other than the seasonal cycle), and for those that
47 did, no consistent ozone depletion and recovery time series was used. In contrast, in the
48 most recent CMIP5 (CMIP phase 5) all models included time-varying ozone fields, using a
49 broad range of methods (e.g. coupled chemistry climate models, semi-offline calculations,
50 prescribed depletion and recovery; see Eyring et al. (2013) for details). In addition, a large
51 number of CMIP5 models included a well resolved stratosphere (“high-top”), potentially
52 allowing for a better representation of the atmospheric response to polar stratospheric ozone
53 changes (Wilcox et al. 2012). The CMIP5 models, therefore, provide an unprecedented
54 multi-model ensemble to assess the role of ozone recovery on the transient 21st Century
55 Southern Hemisphere climate.

56 Since time-varying ozone is included in all of the CMIP5 simulations, one cannot follow
57 the CMIP3 approach - where models were separated into those with and without varying
58 stratospheric ozone - to bring out the effect of ozone changes (e.g. Son et al. (2008b, 2009)).
59 Instead, we use a different technique: taking advantage of the fact that stratospheric ozone
60 began to decline in the 1970’s, reached a minimum around 2005, and is expected to largely
61 recover by mid-century (Eyring et al. 2013), we define four time periods over which the ozone
62 forcing has very different trends (e.g. pre-ozone depletion, ozone depletion, ozone recovery,
63 post ozone recovery). We also exploit the seasonal cycle of the ozone forcing (Thompson and
64 Solomon 2002; Eyring et al. 2013): the cooling of the stratosphere associated with spring-
65 time stratospheric ozone depletion induces the largest changes in the tropospheric circulation

66 in summer (DJF), where the lagged response is due to the time it takes for the stratospheric
67 signal to reach the lower troposphere (Thompson and Solomon 2002; Polvani et al. 2011b).
68 As in Polvani and Solomon (2012), we exploit the seasonal dependence of the stratospheric
69 ozone forcing to distinguish it from the response to greenhouse-gas forcing (which does not
70 have a seasonal cycle), highlighting the distinct signature of ozone recovery on the Southern
71 Hemisphere climate system.

72 In a nutshell, we demonstrate that the CMIP5 models project a significant delay in
73 summer-time Southern Hemisphere climate change between 2005-2045 due to ozone recov-
74 ery largely canceling the effects of other forcings. The effects of ozone recovery are found in
75 the winds, the hydrological cycle, the near-surface air temperatures, and the sea ice concen-
76 trations. We will additionally show that circulation changes due to ozone depletion between
77 1965-2005 are larger than the changes in any scenario over the entire 21st Century.

78 2. Data & Methods

79 *a. CMIP5 climate models and scenarios*

80 We use model output from the CMIP5 archive. Specifically, we analyze monthly-mean,
81 zonal-mean zonal wind, 2 meter air temperature, sea ice concentration, precipitation and
82 evaporation from four forcing scenarios: Historical (1900-2005), RCP2.6, RCP4.5 and RCP8.5
83 (2006-2099). The RCP2.6, RCP4.5 and RCP8.5 (Representative Concentration Pathways)
84 scenarios correspond to futures with varying levels of anthropogenic emissions. RCP2.6 is
85 an aggressive mitigation scenario, where emissions of GHG and the total radiative forcing

86 at the top of the atmosphere stops increasing near 2050 (maximum value of 3.0 W/m^2) and
87 declines to 2.6 W/m^2 by 2100. RCP4.5 is a stabilization scenario, where emissions of GHG
88 are constant after 2150, however, emission increases (and the total radiative forcing) level-off
89 substantially after 2075 (emissions of CO_2 increase at only 40% of their 2005-2050 rate; see
90 Table 4 of Meinshausen et al. (2011)) and the radiative forcing reaches 4.5 W/m^2 by 2100.
91 RCP8.5 is the transient scenario with the largest radiative forcing of 8.5 W/m^2 by 2100
92 which continues to increase thereafter. Additional details about each scenario can be found
93 in Meinshausen et al. (2011).

94 We analyze the three RCPs, rather than just one, (1) to quantify the relative importance
95 of stratospheric ozone recovery across a range of possible futures, and (2) to exploit the fact
96 that since the magnitude and timing of stratospheric ozone changes are similar across all
97 of the RCPs, any difference in the climate responses can be directly attributed to forcings
98 other than ozone. Conversely, trends that are found to be very similar across all RCPs are
99 likely the fingerprint of stratospheric ozone. Therefore, exploration of the different RCPs
100 allows us to bring out the ozone recovery signal.

101 For the sake of brevity, we analyze one ensemble member from every model that provided
102 monthly-mean data for all four scenarios (18 models for zonal wind; 16 models for the
103 other variables; see Table 1). Although all of the CMIP5 models included some form of
104 stratospheric ozone depletion and recovery, some modeling groups prescribed ozone following
105 the IGAC/SPARC ozone database (Cionni et al. 2011), while others employed interactive
106 chemistry that calculates stratospheric ozone online or semi-offline (see Eyring et al. (2013)
107 for additional details). Here, we are interested in whether a robust signal from ozone recovery
108 is evident in the projections of Southern Hemisphere climate, and thus, we consider *all* of

109 the models regardless of their stratospheric ozone scheme.

110 *b. CMIP3 climate models*

111 We also compare the CMIP5 results with those from the 20C3M (present-day) and A1B
112 (future warming) model integrations from CMIP3 (Meehl et al. 2007). Those models are
113 separated into two categories, those with time-varying ozone in both the 20C3M and A1B
114 simulations (varyO3; 11 models) and those with fixed ozone (other than the seasonal cycle)
115 in both simulations (fixO3; 7 models) (see Table 2). Our categories are identical to those
116 in Son et al. (2010), except that we have omitted CNRM CM3 due to some confusion as to
117 whether time-varying ozone was or was not included (see discussion in Son et al. (2010)).

118 *c. Choice of time periods*

119 To bring out the ozone signal, all time series are divided into four time periods: (1)
120 historical (HIST; 1900-1970), (2) ozone depletion (O3DEPL; 1970-2005), ozone recovery
121 (O3RCVR; 2005-2045) and the end of the 21st Century (FUTR; 2045-2099) when ozone
122 has largely recovered and GHG emissions dominate the climate forcing. These four periods
123 naturally emerge from the data analysis (as will be described), but their definitions are also
124 supported by considering the evolution of October stratospheric ozone over the Southern
125 Hemisphere polar cap (see Eyring et al. (2013); Figure 6f): stratospheric ozone begins to
126 decline in the 1970's, reaches a minimum at 2005, and recovers to its 1980 level by 2040
127 to 2045 in the IGAC/SPARC ozone data base and in models with interactive chemistry.
128 It should be clear that the qualitative results of this study are not sensitive to the exact

129 definition of the four periods.

130 *d. Analysis methods*

131 In the following analysis, the jet position is defined, for each month, as the latitude of
132 maximum 700-850 hPa zonal-mean zonal wind, following the method of Barnes and Polvani
133 (2013). For the multi-model mean fields, data from each model simulation is interpolated to
134 a 2° by 2° latitude-longitude grid before plotting. The meridional extent of the dry zone is
135 defined, for each month, as the latitude of the zero-crossing between 30° - 60° S of the zonal-
136 mean precipitation minus evaporation profile. For both the jet position and the dry zone
137 edge, the zonal-mean model data is interpolated using a cubic spline to a 0.1° grid before
138 the final calculation.

139 Plotted time series are smoothed using a 10-year moving-average filter with time step
140 of 1 year. We have performed similar analysis with un-smoothed data and the smoothing
141 is not essential to the conclusions of this study. The best-fit slopes of the time series are
142 calculated from the individual smoothed model data using linear least-squares regression,
143 and the bounds on the slopes denote the symmetric 95% confidence interval. Note that the
144 10-year smoothing causes the O3DEPL period (1970-2005) to include data from 2006-2010,
145 when the different RCPs begin to diverge. Thus, trends during the O3DEPL period differ
146 slightly depending on the RCP used in the smoothing.

3. Seasonal shifts of the circulation

The position of the Southern Hemisphere midlatitude jet stream determines the path of storms and drives ocean circulations and sea-ice dispersion, and stratospheric ozone depletion is known to cause a poleward shift of the Southern Hemisphere jet in summer. As for previous generations of climate models (Kidston and Gerber 2010), the CMIP5 models exhibit an up to 8° equatorward bias of the Southern Hemisphere jet stream position (Barnes and Polvani 2013; Ceppi et al. 2012). Thus, we define for each model simulation the “relative jet position” as the latitude of the jet with respect to its average 1900-1910 latitude. By plotting the relative position of the jet (shift) over time between 1900-2100 in each model, and then averaging the results together in Fig. 1, we avoid the difficulty of model spread masking the coherent poleward jet shift.

Four distinct time periods naturally emerge from the time series of jet position in Fig. 1 (which represents the multi-model mean): (1) historical (HIST; 1900-1970), (2) ozone depletion (O3DEPL; 1970-2005), (3) ozone recovery (O3RCVR; 2005-2045) and (4) GHG dominated (FUTR; 2045-2099). Throughout the HIST period, the jet position remains relatively unchanged, but a sharp southward-shift is evident during the O3DEPL period, with the multi-model mean showing a -1.78° shift of the jet in DJF in RCP8.5 (see Table 3): this number is in excellent agreement with previous studies (see Table 2 of Polvani et al. (2011b)).

If the large poleward shift of the jet during O3DEPL were primarily due to GHG emissions (which are increasing over this period for all scenarios), one would expect the poleward trend in the jet position to continue into the 21st Century. Instead, the trend in jet position

169 halts abruptly around 2005, providing strong evidence that ozone recovery is canceling the
170 influence of GHG emissions between 2005 to 2045 (Arblaster et al. 2011; Polvani et al. 2011a;
171 McLandress et al. 2011). Similar conclusions are reached by Bracegirdle et al. (2013), who
172 show that the RCP8.5 and RCP4.5 multi-model mean jet position exhibits reduced poleward
173 trends between 2000-2049 compared to 1960-1999 in the three Southern Hemisphere ocean
174 basins.

175 The relative amount of cancellation between ozone recovery and GHGs can be seen
176 by comparing the different RCPs during the O3RCVR period. The piece-wise linear-least
177 squares slopes over each time period are plotted in red in Fig. 1, with the slopes given
178 in units of degrees per decade (deg./dec.) in the upper right-hand corner of each panel.
179 The red lines are shifted from the thick black lines for clarity. RCP2.6 shows the smallest
180 negative slope during O3RCVR (-0.04 deg./dec; which is not statistically different from zero)
181 indicative of its smallest, but still increasing, GHG emissions. RCP4.5 exhibits a slightly
182 negative trend (-0.07 deg./dec.) and RCP8.5 exhibits a slightly more negative trend (-0.13
183 deg./dec.), consistent with the larger emissions. Note that while RCP4.5 and RCP8.5 show
184 the jet shifting poleward during O3RCVR, the negative slopes are significantly smaller than
185 those seen during O3DEPL (approximately -0.5 deg./dec.).

186 The varying amounts of cancelation of the poleward shift induced by GHGs among the
187 different RCPs during O3RCVR confirms that GHGs are inducing a poleward trend in the
188 circulation during the O3RCVR period, otherwise the trends among the RCPs would be
189 similar. The small magnitudes of the trends during O3RCVR compared to the O3DEPL
190 and FUTR periods, however, suggest that the influence of GHGs is being opposed by ozone
191 recovery during O3RCVR. This conclusion may appear to conflict with that of Chang et al.

192 (2012), where they report no offset in the poleward migration of the DJF 250 hPa storm
193 tracks over the first half to the 21st Century under RCP8.5 or RCP4.5. This difference,
194 however, may be explained by the magnitude of the trends. The key message is that the
195 projected trends will be smaller in 2005-2045 than in 1960-2005: ozone recovery will delay
196 the poleward migration of the summer-time Southern Hemisphere jet over the next 30 years.
197 After 2050, the importance of GHG emissions is evident, with RCP8.5 showing a continuation
198 of the poleward shift, RCP4.5 showing no change in the jet position, and RCP2.6 showing
199 the jet beginning to recover and return to its Historical position as emissions are reduced.

200 The seasonal differences in the jet position trends provide further evidence that strato-
201 spheric ozone recovery is the forcing responsible for canceling the GHG-induced trends be-
202 tween 2005-2045. Fig. 2 shows similar time series but for winter (JJA), where the winter-time
203 jet position shows no statistically significant trend before 2000, and then exhibits the same
204 negative trend (≈ -0.25 deg./dec.) over the entire 21st Century in RCP8.5. The reduced
205 trend projected in DJF over the O3RCVR period is absent in JJA. Note, however, GHGs
206 and other forcings yield no JJA trends in the O3DEPL period: since these other forcings
207 are likely not seasonal, this further suggests that the DJF trends in the models are largely
208 due to ozone. This is additionally supported by the fact that the FUTR trend in JJA and
209 DJF are not statistically different RC8.5 (≈ -0.3 deg./dec.) or RCP4.5 (\approx zero), and to a
210 lesser extent RCP2.6, highlighting that circulation trends not driven by ozone are similar
211 throughout the two seasons. This further supports our conclusion that the reduced DJF
212 trends between 2005-2045 are due to stratospheric ozone recovery.

213 Vertical cross-sections of the zonal wind changes provide evidence of a stratospheric polar
214 influence, however, multi-model mean fields can skew the relative trends since some models

215 exhibit large biases in the mean jet position. Because of this, in Fig. 3 we show the change
216 in the DJF multi-model mean zonal-mean zonal winds, between the beginning and end of
217 each period (difference between the edges of the period; see Table 3), as a function of relative
218 latitude about the jet position at the start of the period. During O3DEPL (Fig. 3a-c), the
219 positive zonal wind trends extend upward and poleward toward the region of stratospheric
220 ozone depletion as was shown by Polvani et al. (2011b) using a model where only ozone
221 varied. This leaves little doubt that the trends during this period are largely due to polar
222 stratospheric ozone depletion. During the O3RCVR period (Fig. 3d-f), the trends are very
223 weak, and appear instead in the subtropical upper troposphere (approximately 30° north of
224 the jet, or a latitude of 20° S), likely reflecting a response to GHG-induced tropical warming
225 (see for example, Polvani et al. (2011b)). During the FUTR period (Fig. 3g), RCP8.5
226 exhibits trends indicating a poleward (southward) jet shift, although the tropospheric wind
227 trends are weaker than they were during O3DEPL. In RCP4.5 (Fig. 3h), there is a small
228 barotropic increase in the subtropical winds over the FUTR period, while RCP2.6 (Fig.
229 3i) exhibits a clear reversal of the midlatitude trends with the jet shifting *equatorward*.
230 This result indicates that if GHG emissions are very aggressively reduced, the atmospheric
231 circulation will begin to relax back to its pre-ozone hole position towards the end of this
232 century.

233 4. Results from CMIP3

234 Further evidence that the reduced trends during the O3RCVR period are due to cancella-
235 tion of GHG-induced changes by ozone recovery is found in the CMIP3 model output. Some

236 of the CMIP3 models did not include ozone depletion and recovery, while others did, and
237 building on previous work (Son et al. 2008a, 2009), we use these ozone differences to extract
238 the signature of ozone depletion and recovery on future circulation trends by grouping the
239 CMIP3 models into those with time-varying ozone (varyO3) and those without (fixO3).

240 Fig. 4 shows the time series of jet position from the 20th Century and A1B experiments
241 of the CMIP3 models. The trends for the varyO3 models (Fig. 4a) are most similar to
242 those of the CMIP5 RCP8.5 simulations (Fig. 1a), with ozone depletion inducing a -1.5°
243 shift of the jet, and ozone recovery canceling GHG-induced circulation trends, yielding an
244 insignificant trend in the jet position between 2005-2045. The fixO3 models tell a different
245 story (Fig. 4b), with the future trends in jet position across all three periods being statisti-
246 cally indistinguishable from one another at 95% confidence (calculated using a comparison
247 of means).

248 The trends at the end of the 21st Century (when ozone has recovered) in varyO3 and fixO3
249 are statistically the same (≈ -0.2 deg./dec.), confirming that non-ozone forced circulation
250 trends are similar across the two model groups. This supports our conclusion that differences
251 between the trends during the O3DEPL and O3RCVR periods are due to the addition
252 and cancellation of wind trends caused by ozone depletion and recovery. Furthermore, the
253 jet position trends during O3DEPL are statistically the same between the CMIP3 varyO3
254 integrations and the CMIP5 RCP's (≈ -0.5 deg./dec.), further strengthening the quantitative
255 projections of the CMIP models.

5. Shifts in the subtropical dry zones

The cancellation of GHG-induced climate trends by ozone recovery is also found in another important measure of the atmospheric circulation: the extent of the subtropical dry zones. The expansion of the atmospheric overturning circulation (Hadley cell), and concurrent expansion of the subtropical dry zones has been documented in the observations (Seidel et al. 2008; Fu et al. 2006), and modeling studies suggest such a trend can be induced by increasing GHG emissions and/or stratospheric ozone depletion (Lu et al. 2009; Polvani et al. 2011b; McLandress et al. 2011). Scheff and Frierson (2012a) show that the CMIP5 models robustly exhibit a poleward expansion of the subtropical dry zones between the end of the 20th and 21st Centuries, and we extend their analysis by looking year-by-year at the trends in the DJF dry zone edge.

As seen in Fig. 5, the largest trends in the subtropical dry zone extent occur during the O3DEPL and FUTR periods. Statistically insignificant trends are present during O3RCVR, when ozone recovery largely cancels the effects of GHG emission increases. The dry zones continue to expand in RCP8.5 during the FUTR period (Fig. 5a), level-off in RCP4.5 (Fig. 5b) and rebound toward their historical positions in RCP2.6 (Fig. 5c). Trends in the dry zone edge for JJA (not shown) give similar poleward slopes in both the O3DEPL and O3RCVR periods, confirming that differences in the trends over these two periods are confined to DJF.

We wish to emphasize that, while the midlatitude jet position is computed using the lower-tropospheric zonal-mean zonal winds, the dry zone edge is computed using the moisture fluxes, namely, where the zonal-mean precipitation minus evaporation is zero (see Section 2). Thus, the strong similarities between the jet trends and dry zone edge trends between

278 1900 and 2100 (Fig. 1 and Fig. 5) are not due to the fact that we are using similar model
279 diagnostics: rather, they confirm a broad hemispheric-wide response of the circulation to
280 stratospheric ozone depletion and recovery. These similarities also support the conclusions
281 of Scheff and Frierson (2012b), whereby the shifts in the hydrological cycle are coupled to
282 the simultaneous poleward shift of the Hadley cell edge with the midlatitude storm tracks
283 and jet.

284 **6. Seasonality of the circulation trends**

285 The seasonality of stratospheric ozone depletion and recovery is documented extensively
286 in the model-based literature (see, for example, Eyring et al. (2013)). We exploit this
287 seasonality to provide further evidence that the reduced trends in the period 2005-2045 are
288 largely due to stratospheric ozone recovery canceling the effects of GHG increases. Fig.
289 6a shows the total shift in the jet latitude as a function of month and time period for
290 RCP8.5; similarly, Fig. 6b shows the shift in the subtropical dry zone edge. During the
291 O3DEPL period (1970-2005; red curves), the largest poleward shifts are found in the summer,
292 when spring-time stratospheric ozone depletion induces the largest tropospheric response; no
293 consistent trend among the models is found during the winter months, as previously shown.
294 During the O3RCVR period (2005-2045; black curves), most models exhibit a poleward
295 shift of the jet and dry zone edge outside of the summer months. The near zero multi-model
296 mean shift during summer confirms that ozone recovery is canceling the GHG-induced shift
297 in DJF. When ozone has largely recovered (2045-2100; blue curves), there is less seasonal
298 variation in the trends of the jet and subtropical dry zone positions. This further supports

299 the conclusion that the seasonality of the trends during the O3DEPL period cannot be due
300 to GHGs alone, as these influence the circulation year-round. Note that the seasonality of
301 trends in Fig. 6a is clearer than Fig. 6b, since the ozone signal weakens with distance from
302 the pole as noted by Polvani et al. (2011b).

303 7. Seasonal surface temperature trends

304 Bitz and Polvani (2012) studied the effects of stratospheric ozone depletion on South-
305 ern Hemisphere surface temperatures using an ocean-eddy resolving coupled climate model,
306 and found that the annual-mean mid-to-high latitude surface temperatures warmed with
307 ozone depletion. The opposite response is expected to follow from the projected recovery of
308 stratospheric ozone, as suggested by the results of Smith et al. (2012). In this section we
309 investigate whether a surface temperature response to ozone depletion and recovery can be
310 identified in the Southern Hemisphere climate in CMIP5.

311 The RCP8.5 simulations show a monotonic increase of 2-meter (2m) air temperature
312 over the Southern Ocean (46°-90° S) in the annual mean (Fig. 7a), with the warming
313 trends increasing steadily with time over the next century. The summer and winter months,
314 individually, also show increasing temperature trends over the next century (not shown).
315 Since the warming over the 21st Century does not appear to slow down during O3RCVR,
316 we are unable to extract the ozone signal from near-surface temperatures directly.

317 A surface temperature signal from stratospheric ozone recovery is apparent, however,
318 when the seasonal cycle of the trends is considered. Fig. 6c shows the monthly change in
319 mid-to-high latitude (46°-90° S) 2m air temperatures. The overall positive trends in Fig.

320 6c indicate that the 2m air temperatures are warming throughout the year. However, note
321 that during O3DEPL (red curve), the winter months (JAS) warm more than the summer
322 months (JFM). This preference for warming during the winter relative to summer is also
323 evident over the FUTR period. In contrast, only a weak seasonal signal is present over the
324 O3RCVR period.

325 This seasonal cycle of the warming can be exploited to extract the surface warming signal
326 in O3DEPL relative to O3RCVR. We define the *seasonal amplitude* of the 2m air tempera-
327 ture as the difference between the mean summer-time (JFM) and winter-time temperatures
328 (JAS). This quantity is always positive, since the summer is on the order of 7°C warmer
329 than the winter in the models. Note that the seasonal temperature response in Fig. 6c is
330 lagged by one month (smallest O3DEPL trends in Jan.) compared to the jet and dry-zone
331 edge responses (Fig. 6a,b; smallest O3DEPL trends in Dec.), supporting the use of JFM
332 and JAS, rather than DJF and JJA as done in the previous sections.

333 Fig. 7b shows the changes in the seasonal amplitude of 2m air temperature in RCP8.5:
334 these changes exhibit similar signatures of ozone depletion and recovery as previously dis-
335 cussed for other quantities (Fig. 1 and Fig. 5). Negative trends imply that the winter is
336 warming more than the summer (the difference between the winter and summer tempera-
337 tures is decreasing) and the winter warms more than the summer in all three future periods.
338 However, the O3RCVR exhibits smaller negative trends in seasonal amplitude compared to
339 the O3DEPL and FUTR periods, providing evidence that ozone depletion may have induced
340 a greater warming of winter relative to summer over the O3DEPL period, and that ozone
341 recovery may mitigate future winter warming relative to the summer.

342 In order to mechanistically understand the role of ozone depletion and recovery on the

343 trends in the seasonal amplitude of 2m temperature, we show latitude-longitude plots of its
344 multi-model mean change (end of period minus beginning of period) in Fig. 8 for the three
345 RCPs. Looking first at O3DEPL (Fig. 8a-c), an annular pattern emerges, with a decrease in
346 the seasonal amplitude (blue shading; warming of the winter relative to the summer) confined
347 poleward of 46° S (solid black line), and an increase in the seasonal amplitude (yellow and
348 red shading; cooling of winter relative to the summer) equatorward of 46° S. While we
349 are unaware of previous studies explicitly showing the accelerated surface warming of the
350 winter relative to summer induced by ozone depletion, or the effects of ozone recovery on the
351 seasonal warming signal, the mechanism behind the seasonal response of surface temperature
352 from stratospheric ozone depletion has been previously suggested (Sigmond and Fyfe 2010;
353 Bitz and Polvani 2012; Smith et al. 2012); we briefly summarize it here.

354 During the O3DEPL period, stratospheric cooling in the spring-time from ozone loss
355 induces a poleward shift of the midlatitude winds during summer. The shift of the summer-
356 time near-surface winds both warms the ocean surface by mixing warmer waters up from
357 below and by inducing an anomalous meridional overturning circulation which transports
358 cold, high-latitude surface water equatorward, and warm, low-latitude surface water pole-
359 ward. Thus, in summer during O3DEPL, the ocean surface is warmer equatorward of the jet
360 compared to poleward of the jet. In winter during O3DEPL, although the wind anomalies
361 are no longer present, the ocean surface remains anomalously warm due to the long oceanic
362 timescales. In addition to the ocean anomalies themselves, a warmer ocean surface leads to
363 basal melting and a reduction in sea-ice growth, which allows for increased surface absorption
364 of short wave fluxes in summer. This anomalous energy input into the ocean is released to
365 the atmosphere during winter when the air-sea temperature difference is maximized, further

366 increasing the high-latitude winter air temperatures relative to summer (Manabe and Stouffer
367 fer 1980; Manabe et al. 1992; Bitz and Polvani 2012; Dwyer et al. 2012). Putting all of this
368 together, the high-latitude warming in winter is larger than in summer, and the low-latitude
369 warming in winter is smaller than in summer, creating a dipolar pattern of the seasonal
370 amplitude trends during the O3DEPL period (Fig. 8a-c).

371 This mechanism suggests that during the ozone depletion period, anomalous surface air
372 temperatures are driven by anomalous ocean temperatures which, in turn, are driven by
373 shifts in the atmospheric circulation. In support of the role of the atmospheric circulation
374 driving the air temperature trends, we overlay the 1960-1970 multi-model mean jet latitude
375 (46° S) as a black line in all panels of Fig. 8; the seasonal amplitude trend pattern aligns well
376 with the latitude of the jet during O3DEPL. In addition, as ozone recovers between 2005-
377 2045, the jet shift is reduced in all RCPs (Fig. 1) and one might expect this to reduce the
378 trends in the seasonal amplitude during O3RCVR. Indeed, trends during O3RCVR shown in
379 Fig. 8d-f are weaker, and there is less model agreement than during O3DEPL. In addition,
380 RCP2.6 exhibits the smallest circulation trends during the O3RCVR period (Fig. 1 and Fig.
381 5) and also exhibits the smallest change in seasonal amplitude among the RCPs during this
382 period (Fig. 8f).

383 We conclude this section by discussing the FUTR period, when stratospheric ozone has
384 largely recovered. The patterns of the trends in 2m air temperature for the FUTR period are
385 shown in Fig. 8g-i. For RCP4.5, the circulation response is weak in the FUTR period, and
386 similarly, so are the changes in the seasonal amplitude. For RCP2.6, although model agree-
387 ment is low, the sign of the changes in seasonal amplitude have reversed during the FUTR
388 period compared to the O3DEPL period in most locations except for east of the Weddell Sea.

389 This is consistent with the circulation beginning to recover during this period. Finally, for
390 RCP8.5, the trend patterns and magnitudes appear similar to those during O3DEPL (Fig.
391 8a). However, during the FUTR period, the response of the seasonal amplitude cannot be
392 easily explained by the ocean circulation and mixing mechanism described above, since the
393 GHG-induced wind anomalies occur year-round (Fig. 6a; blue line) and the mechanism re-
394 quires that the wind anomalies occur in the summer only (as is the case for ozone depletion).
395 We do not know why the trend pattern over the FUTR period is so similar to that over the
396 O3DEPL, but previous studies suggest that the high-latitude accelerated warming of winter
397 relative to summer with increased GHG concentrations can be explained by the changes in
398 air-sea fluxes associated with sea ice loss (Manabe and Stouffer 1980; Manabe et al. 1992;
399 Dwyer et al. 2012). It is also possible that seasonal differences in the wind strength response
400 could cause the seasonal amplitude patterns in Fig. 8g-i, however, determining what drives
401 the midlatitude increase in the seasonal amplitude between 2045-2100 is beyond the scope
402 of this study.

403 **8. Antarctic sea ice trends**

404 As described in the previous section, ozone depletion warms the ocean surface through
405 changes in the tropospheric winds, and this ocean warming limits sea ice growth. The
406 response of sea ice concentrations to ozone depletion and recovery can be seen in the time
407 series of the JFM sea ice area (Fig. 9) in RCP8.5. The largest decrease in sea ice area
408 occurs during the O3DEPL period, when high latitude warming both melts the sea ice and
409 the anomalous surface wind stress (from the jet shift) transports the ice away from the

410 continent (Sigmond and Fyfe 2010; Bitz and Polvani 2012). This modeled Antarctic sea
411 ice decrease in the last three decades is at odds with observations, which show a small yet
412 statistically significant increase in sea ice extent (Liu et al. 2004; Holland and Kwok 2012;
413 Turner et al. 2013). The difference remains unexplained, however, a recent study by Polvani
414 and Smith (2013) suggests that this discrepancy may be explained by internal variability
415 since the observed trends fall within the bounds of the natural variability of the system.

416 Contrasting the JFM and JAS panels in Fig. 9, one can see that the relative changes
417 in sea ice area, in O3DEPL, are much stronger in JFM than in JAS, in agreement with
418 Sigmond and Fyfe (2010). In the coming decades, however, the CMIP5 models project that
419 ozone recovery will mitigate the effects of increasing GHGs on summer Antarctic sea ice.
420 This can be seen from the fact that the rate of JFM sea ice loss over the O3RCVR period
421 is nearly half of that during O3DEPL, in agreement with Smith et al. (2012).

422 9. Conclusions

423 We have demonstrated, using transient climate simulations from 18 CMIP5 models, that
424 stratospheric ozone recovery will be a major driver of Southern Hemisphere climate over
425 the 21st Century. Focusing on specific time periods based on the trends in stratospheric
426 ozone forcing, and exploiting the seasonality of ozone depletion and recovery to separate the
427 ozone signal from that of other climate forcings, we have shown that the CMIP5 models
428 clearly project delayed climate change over the entire Southern Hemisphere in summer as a
429 consequence of ozone recovery. This reduced climate change manifests itself in the summer-
430 time Southern Hemisphere winds, dry zone edge, surface temperatures and Antarctic sea ice

431 concentrations. To further elucidate the contribution of stratospheric ozone depletion and
432 recovery on the summer-time tropospheric trends over the 21st Century, we compare results
433 from three different forcing scenarios (RCP8.5, RCP4.5 and RCP2.6) and demonstrate the
434 respective cancelation between the trends driven by stratospheric ozone and those driven by
435 increasing GHG emissions across a range of climate scenarios.

436 These results highlight the perhaps surprising fact that the changes in the simulated
437 summer-time tropospheric circulation between 1970-2005, driven largely by stratospheric
438 ozone depletion, are of comparable magnitude (or larger) than the projected changes in *any*
439 scenario over the entire 21st Century (see Table 3). Previous studies based on targeted
440 model experiments using a single model (Arblaster and Meehl 2006; Polvani et al. 2011a;
441 McLandress et al. 2011) have suggested ozone recovery would cancel a significant portion of
442 the GHG-induced changes between 2000-2045. Our study supports this conclusion, show-
443 ing that the transient future simulations from 18 CMIP5 models exhibit delayed Southern
444 Hemisphere climate change as a consequence of ozone recovery. In addition, the CMIP5
445 future “best-case” emissions scenario (RCP2.6), where GHG emissions decrease throughout
446 the late 21st Century, demonstrates that by 2100 the circulation rebounds only 40% of the
447 distance caused by 20th Century ozone depletion (Fig. 1c). Finally, while the most robust
448 response to future climate change is a warming over the Earth’s surface, our results suggest
449 that ozone recovery may modify the seasonal fingerprint of the temperature signal over the
450 first half of the 21st Century.

451 *Acknowledgments.*

452 We acknowledge Haibo Liu for obtaining the CMIP5 data and Darryn Waugh for helpful
453 discussions and three anonymous reviewers for their helpful comments. We acknowledge
454 the World Climate Research Programme’s Working Group on Coupled Modelling, which is
455 responsible for CMIP, and we thank the climate modeling groups for producing and mak-
456 ing available their model output. For CMIP the U.S. Department of Energy’s Program for
457 Climate Model Diagnosis and Intercomparison provides coordinating support and led de-
458 velopment of software infrastructure in partnership with the Global Organization for Earth
459 System Science Portals. EAB is funded by a NOAA Climate & Global Change Fellowship
460 through the University Corporation of Atmospheric Research Visiting Science Program.
461 LMP is funded, in part, by a grant of the U.S. National Science Foundation to Columbia
462 University.

REFERENCES

- 465 Arblaster, J. M., G. a. Meehl, and D. J. Karoly, 2011: Future climate change in the South-
466 ern Hemisphere: Competing effects of ozone and greenhouse gases. *Geophysical Research*
467 *Letters*, **38 (2)**, L02701, doi:10.1029/2010GL045384.
- 468 Arblaster, J. M. and G. A. Meehl, 2006: Contributions of external forcings to Southern
469 Annular Mode trends. *J. Climate*, **19**, 2896–2905.
- 470 Barnes, E. A. and L. M. Polvani, 2013: Response of the midlatitude jets and of their vari-
471 ability to increased greenhouse gases in the CMIP5 models. *J. Climate*, **in press**.
- 472 Bitz, C. M. and L. M. Polvani, 2012: Antarctic climate response to stratospheric ozone
473 depletion in a fine resolution ocean climate model. *Geophysical Research Letters*, **39 (20)**,
474 L20705, doi:10.1029/2012GL053393, .
- 475 Bracegirdle, T. J., E. Shuckburgh, J.-B. Sallee, Z. Wang, A. J. S. Meijers, N. Bruneau,
476 T. Phillips, and L. J. Wilcox, 2013: Assessment of surface winds over the Atlantic, Indian,
477 and Pacific Ocean sectors of the Southern Ocean in CMIP5 models: historical bias, forcing
478 response, and state dependence. *J. Geophys. Res.*, **118**, 547–562, doi:10.1002/jgrd.50153.
- 479 Ceppi, P., Y. Hwang, D. Frierson, and D. Hartmann, 2012: Southern Hemisphere jet lat-
480 itude biases in CMIP5 models linked to shortwave cloud forcing. *Geophys. Res. Lett.*,
481 **39 (October)**, 1–5, doi:10.1029/2012GL053115.

482 Chang, E. K. M., Y. Guo, and X. Xia, 2012: CMIP5 multimode ensemble projection of
483 storm track change under global warming. *J. Geophys. Res.*, **117**, D23118, doi:0.1029/
484 2012JD018578.

485 Cionni, I., et al., 2011: Ozone database in support of CMIP5 simulations: results and
486 corresponding radiative forcing. *Atmospheric Chemistry and Physics*, **11** (21), 11267–
487 11292, doi:10.5194/acp-11-11267-2011, .

488 Cordero, E. C. and P. M. d. F. Forster, 2006: Stratospheric variability and trends in models
489 used for the IPCC AR4. *Atmos. Chem. Phys.*, **6**, 53695380.

490 Dwyer, J. G., M. Biasutti, and A. H. Sobel, 2012: Projected Changes in the Seasonal
491 Cycle of Surface Temperature. *Journal of Climate*, **25** (18), 6359–6374, doi:10.1175/
492 JCLI-D-11-00741.1.

493 Eyring, V., et al., 2013: Long-term ozone changes and associated climate impacts in CMIP5
494 simulations. *J. Geophys. Res.*

495 Fu, Q., C. Johanson, J. Wallace, and T. Reichler, 2006: Enhanced mid-latitude tropospheric
496 warming in satellite measurements. *Science*, **312**, .

497 Holland, P. R. and R. Kwok, 2012: Wind-driven trends in antarctic sea-ice drift. *Nat. Geosci.*,
498 **5**, 872–875, doi:10.1038/NGEO1627.

499 Kang, S. M., L. M. Polvani, J. C. Fyfe, and M. Sigmond, 2011: Impact of polar ozone
500 depletion on subtropical precipitation. *Science*, **332**, 951–954.

501 Kidston, J. and E. Gerber, 2010: Intermodel variability of the poleward shift of the austral

502 jet stream in the CMIP3 integrations linked to biases in the 20th century climatology.
503 *Geophys. Res. Lett.*, **37**, L09 708, doi:10.1029/2010GL042873.

504 Lee, S. and S. B. Feldstein, 2013: Detecting Ozone- and Greenhouse Gas-Driven Wind Trends
505 with Observational Data. *Science*, **339 (6119)**, 563–567, doi:10.1126/science.1225154, .

506 Liu, J., J. Curry, and D. Martinson, 2004: Interpretation of recent Antarctic sea ice vari-
507 ability. *Geophysical Research Letters*, **31 (2)**, L02 205, doi:10.1029/2003GL018732.

508 Lu, J., C. Deser, and T. Reichler, 2009: Cause of the widening of the tropical belt since
509 1958. *Geophysical Research Letters*, **36 (3)**, L03 803, doi:10.1029/2008GL036076.

510 Manabe, S., M. Spelman, and R. Stouffer, 1992: Transient responses of a coupled ocean-
511 atmosphere model to gradual changes of atmospheric CO₂. Part II: Seasonal response. *J.*
512 *Climate*, **5**, 105–126, .

513 Manabe, S. and R. Stouffer, 1980: Sensitivity of a global climate model to an increase of CO
514 2 concentration in the atmosphere. *Journal of Geophysical Research*, **85 (80)**, 5529–5554.

515 McLandress, C., T. G. Shepherd, J. F. Scinocca, D. a. Plummer, M. Sigmond, A. I. Jonsson,
516 and M. C. Reader, 2011: Separating the Dynamical Effects of Climate Change and Ozone
517 Depletion. Part II: Southern Hemisphere Troposphere. *J. Climate*, **24 (6)**, 1850–1868,
518 doi:10.1175/2010JCLI3958.1, .

519 Meehl, G. A., C. Covey, T. Delworth, M. Latif, B. McAvaney, J. F. B. Mitchell, R. J.
520 Stouffer, and K. E. Taylor, 2007: The WRCM CMIP3 multi-model dataset: A new era in
521 climate change research. *Bull. Amer. Meteor. Soc.*, **88**, 1383–1394.

522 Meinshausen, M., et al., 2011: The RCP greenhouse gas concentrations and their extensions
523 from 1765 to 2300. *Climate Change*, **109 (1-2)**, 213–241, doi:10.1007/s10584-011-0156-z,
524 .

525 Polvani, L. M. and K. L. Smith, 2013: Can natural variability explain observed Antarctic sea
526 ice trends? New modeling evidence from CMIP5. *Geophys. Res. Lett.*, **40**, doi:10.1002/
527 grl.50578.

528 Polvani, L. M. and S. Solomon, 2012: The signature of ozone depletion on tropical tempera-
529 ture trends, as revealed by their seasonal cycle in model integrations with single forcings.
530 *Geophys. Res. Lett.*, **117**, doi:10.1029/2012JD017719.

531 Polvani, L., M. Previdi, and C. Deser, 2011a: Large cancellation, due to ozone recovery, of
532 future Southern Hemisphere atmospheric circulation trends. *Geophys. Res. Lett.*, **38 (Jan-**
533 **uary)**, 1–6, doi:10.1029/2011GL046712, .

534 Polvani, L., D. Waugh, G. Correa, and S. Son, 2011b: Stratospheric ozone depletion: The
535 main driver of twentieth-century atmospheric circulation changes in the Southern Hemi-
536 sphere. *Journal of Climate*, 795–812, doi:10.1175/2010JCLI3772.1, .

537 Roscoe, H. and J. Haigh, 2007: Influences of ozone depletion, the solar cycle and the QBO
538 on the Southern Annular Mode. *Quart. J. Roy. Meteor. Soc.*, **1864**, 1855–1864, doi:10.
539 1002/qj.

540 Scheff, J. and D. Frierson, 2012a: Robust future precipitation declines in CMIP5 largely re-
541 flect the poleward expansion of model subtropical dry zones. *Geophysical Research Letters*,
542 **39 (September)**, 1–6, doi:10.1029/2012GL052910, .

543 Scheff, J. and D. Frierson, 2012b: Twenty-First-Century Multimodel Subtropical Precipitation Declines Are Mostly Midlatitude Shifts. *Journal of Climate*, **25** (12), 4330–4347,
544 doi:10.1175/JCLI-D-11-00393.1, .

546 Seidel, D. J., Q. Fu, W. J. Randel, and T. J. Reichler, 2008: Widening of the tropical belt
547 in a changing climate. *Nat. Geosci.*, **1**, 21–24.

548 Sigmond, M. and J. C. Fyfe, 2010: Has the ozone hole contributed to increased Antarctic
549 sea ice extent? *Geophys. Res. Lett.*, **37** (18), L18 502, doi:10.1029/2010GL044301, .

550 Smith, K. L., L. M. Polvani, and D. R. Marsh, 2012: Mitigation of 21st century Antarctic sea
551 ice loss by stratospheric ozone recovery. *Geophysical Research Letters*, **39** (20), L20 701,
552 doi:10.1029/2012GL053325, .

553 Son, S.-W., S. Lee, S. B. Feldstein, and J. E. T. Hovee, 2008a: Time scale and feedback of
554 zonal-mean-flow variability. *J. Atmos. Sci.*, **65**, 935–952.

555 Son, S.-W., N. F. Tandon, L. M. Polvani, and D. W. Waugh, 2009: Ozone hole and Southern
556 Hemisphere climate change. *Geophysical Research Letters*, **36** (15), L15 705, doi:10.1029/
557 2009GL038671.

558 Son, S., E. P. Gerber, J. Perlwitz, L. M. Polvani, N. Gillett, K. Seo, and coauthors, 2010:
559 The impact of stratospheric ozone on the Southern Hemisphere circulation changes: A
560 multimodel assessment. *J. Geophys. Res.*, **115**, doi:doi:10.1029/2010JD014271.

561 Son, S., L. Polvani, D. Waugh, and H. Akiyoshi, 2008b: The impact of stratospheric ozone
562 recovery on the Southern Hemisphere westerly jet. *Science*, **1486** (2008), doi:10.1126/
563 science.1155939.

564 Thompson, D. W. J., S. Solomon, P. J. Kushner, M. H. England, K. M. Grise, and D. J.
565 Karoly, 2011: Signatures of the Antarctic ozone hole in Southern Hemisphere surface
566 climate change. *Nature Geoscience*, **4** (11), 741–749, doi:10.1038/ngeo1296.

567 Thompson, D. W. and S. Solomon, 2002: Interpretation of recent Southern Hemisphere
568 climate change. *Science*, **296**, 895–899.

569 Turner, J., T. J. Bracegirdle, T. Phillips, G. J. Marshall, and J. S. Hosking, 2013: An
570 Initial Assessment of Antarctic Sea Ice Extent in the CMIP5 Models. *J. Climate*, **26** (5),
571 1473–1484, doi:10.1175/JCLI-D-12-00068.1.

572 Waugh, D. W., F. Primeau, T. Devries, and M. Holzer, 2013: Recent changes in the ven-
573 tilation of the southern oceans. *Science (New York, N.Y.)*, **339** (6119), 568–70, doi:
574 10.1126/science.1225411, .

575 Wilcox, L. J., A. J. Charlton-Perez, and L. J. Gray, 2012: Trends in Austral jet position
576 in ensembles of high- and low-top CMIP5 models. *J. Geophys. Res.*, **117**, D13 115, doi:
577 10.1029/2012JD017597.

578 Wu, Y., R. Seager, M. Ting, N. Naik, and T. Shaw, 2013: Atmospheric circulation response
579 to an instantaneous doubling of carbon dioxide Part I: Model experiments and transient
580 thermal response in the troposphere. *J. Climate*, **in press**.

581 **List of Tables**

582	1	Data availability of CMIP5 model output.	29
583	2	Data availability of CMIP3 model output, distinguishing those models with	
584		fixed stratospheric ozone and those that include time-varying stratospheric	
585		ozone.	30
586	3	Multi-model mean DJF shift (degrees North) of the midlatitude jet position.	
587		Negative values denote a poleward shift and positive values denote an equa-	
588		torward shift. Year ranges below each period denote the edges of the period	
589		(beginning and end) used to calculate changes.	31

model name	zonal wind	2m temp., sea ice precip. & evap.
BCC-CSM1.1	x	x
CanESM2	x	x
CSIRO-Mk3-6-0	x	x
GFDL-CM3	x	x
GFDL-ESM2G	x	x
GFDL-ESM2M	x	x
GISS-E2-H	x	
GISS-E2-R	x	x
HadGEM2-ES	x	x
IPSL-CM5A-LR	x	x
IPSL-CM5A-MR	x	x
MIROC5	x	x
MIROC-ESM	x	x
MIROC-ESM-CHEM	x	x
MPI-ESM-LR	x	x
MPI-ESM-MR	x	
MRI-CGCM3	x	x
NorESM1-M	x	x

TABLE 1. Data availability of CMIP5 model output.

fixed ozone	varying ozone
BCCR-BCM2.0	CSIRO-Mk3.0
CGCM3.1 (T63)	GFDL-CM2.0
GISS-AOM	GFDL-CM2.1
FGOALS-g1.0	GISS-EH
INM-CM3.0	GISS-ER
IPSL-CM4	INGV-SXG
MRI-CGCM2.3.2	ECHAM5/MPI-OM
	CCSM3
	PCM
	UKMO-HadCM3
	UKMO-HadGEM1

TABLE 2. Data availability of CMIP3 model output, distinguishing those models with fixed stratospheric ozone and those that include time-varying stratospheric ozone.

Period	Historical	RCP8.5	RCP4.5	RCP2.6
HIST (1960-1970)-(1900-1910)	-0.21°			
O3DEPL (2000-2010)-(1960-1970)		-1.78°	-1.59°	-1.63°
O3RCVR (2040-2050)-(2000-2010)		-0.16°	-0.19°	-0.02°
FUTR (2089-2099)-(2040-2050)		-1.42°	+0.07°	+0.80°

TABLE 3. Multi-model mean DJF shift (degrees North) of the midlatitude jet position. Negative values denote a poleward shift and positive values denote an equatorward shift. Year ranges below each period denote the edges of the period (beginning and end) used to calculate changes.

List of Figures

- 590
- 591 1 Time series of the CMIP5 Southern Hemisphere DJF jet position relative to
592 the 1900-1910 value over the Historical and three climate scenarios (RCP8.5,
593 RCP4.5 and RCP2.6). Thin black curves denote the individual models and
594 the multi-model mean is plotted in black. Red lines denote the piece-wise
595 linear least-squares slopes, which are also given in the panels above in units of
596 degrees per decade. Time series have been smoothed using a 10-year moving
597 average filter (see Section 2d for details). 34
- 598 2 As in Fig. 1 but for JJA. 35
- 599 3 Multi-model mean change (in m/s per decade) of the DJF zonal-mean zonal
600 winds for three climate scenarios, grouped by period. The change is defined
601 as the difference between the edges of the periods (see Table 3), and the black
602 contours show the zonal-mean zonal wind fields for the earlier edge of each
603 period. The plotting convention is such that the equator (EQ) is to the right
604 and the South Pole (SP) is to the left in each panel. Fields were interpolated
605 to a 2° by 2° latitude-longitude grid before plotting. 36
- 606 4 As in Fig. 1 but for the CMIP3 models, separated by those models (a) with
607 time-varying stratospheric ozone and those (b) with fixed ozone. 37
- 608 5 As in Fig. 1 but for the latitude of the subtropical dry zone edge (precipitation
609 minus evaporation zero-crossing). 38

610 6 (a,b) Shift in the Southern Hemisphere (a) jet and (b) dry zone edge (zero-
611 crossing of precipitation minus evaporation) as a function of month for three
612 time periods over the Historical and RCP8.5 scenarios. (c) Similar to (a,b)
613 but for the area-averaged high-latitude (46° - 90° S) two-meter air temperature.
614 In all panels, the bars denote the 25th-75th percentile range and the crosses
615 denote values outside of this interval. The calculation is done as a time-slice
616 difference, and the years used for each time period are given in Table 3. 39

617 7 As in Fig. 1 but for the RCP8.5 high-latitude (46° - 90° S) 2-meter air tem-
618 perature for (a) the annual-mean and (b) the seasonal amplitude defined as
619 JFM-JAS (summer minus winter). 40

620 8 Multi-model mean change in degrees per decade of the seasonal amplitude
621 of 2-meter air temperatures. Stippling denotes locations where at least 80%
622 of the models (13 of 16) agree on the sign of the change. Solid black lines
623 denote the multi-model mean jet position at the beginning of the O3DEPL
624 period (46° S; see Table 3 for the years included in each period). Fields were
625 interpolated to a 2° by 2° latitude-longitude grid before plotting. 41

626 9 As in Fig. 1 but for the RCP8.5 JFM and JAS percent change in sea ice area. 42

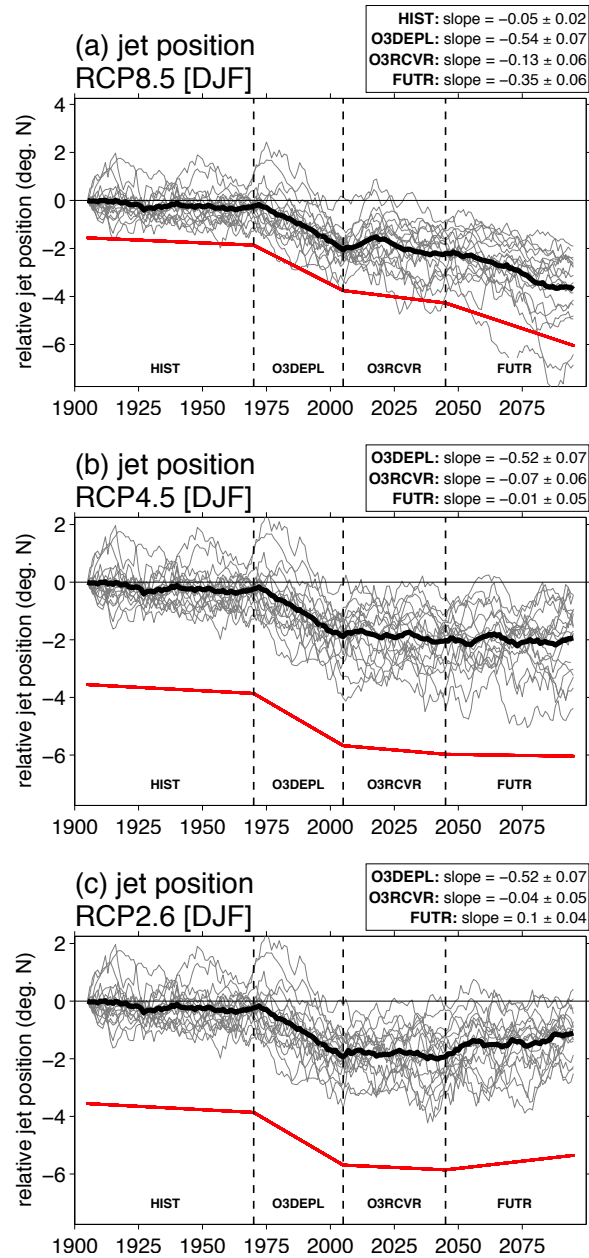


FIG. 1. Time series of the CMIP5 Southern Hemisphere DJF jet position relative to the 1900-1910 value over the Historical and three climate scenarios (RCP8.5, RCP4.5 and RCP2.6). Thin black curves denote the individual models and the multi-model mean is plotted in black. Red lines denote the piece-wise linear least-squares slopes, which are also given in the panels above in units of degrees per decade. Time series have been smoothed using a 10-year moving average filter (see Section 2d for details).

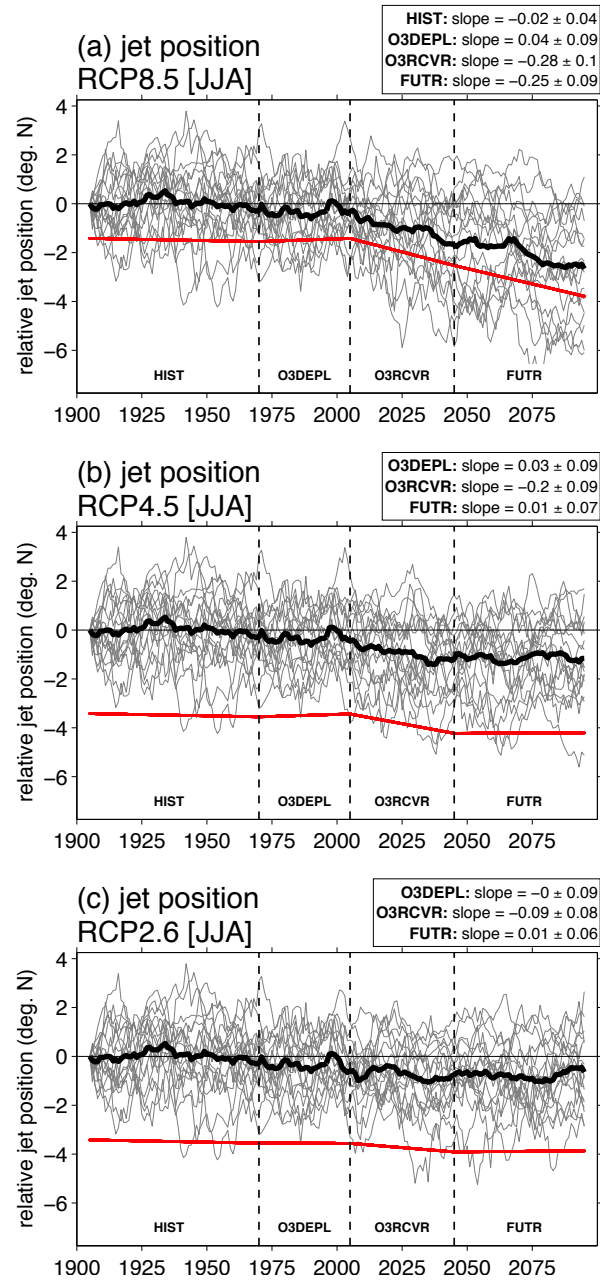


FIG. 2. As in Fig. 1 but for JJA.

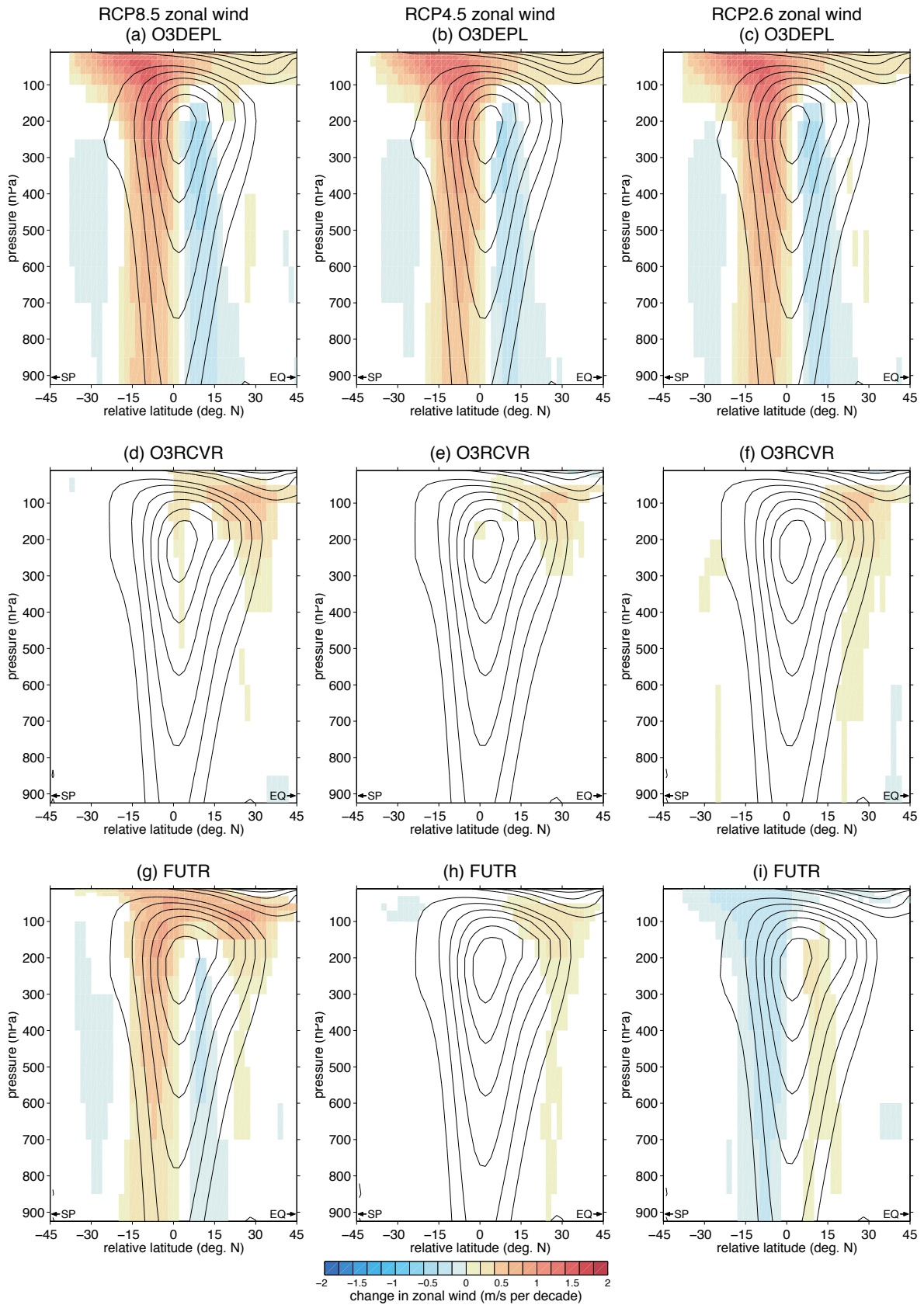


FIG. 3. Multi-model mean change (in m/s per decade) of the DJF zonal-mean zonal winds for three climate scenarios, grouped by period. The change is defined as the difference between the edges of the periods (see Table 3), and the black contours show the zonal-mean zonal wind fields for the earlier edge of each period. The plotting convention is such that the equator (EQ) is to the right and the South Pole (SP) is to the left in each panel. Fields were interpolated to a 2° by 2° latitude-longitude grid before plotting.

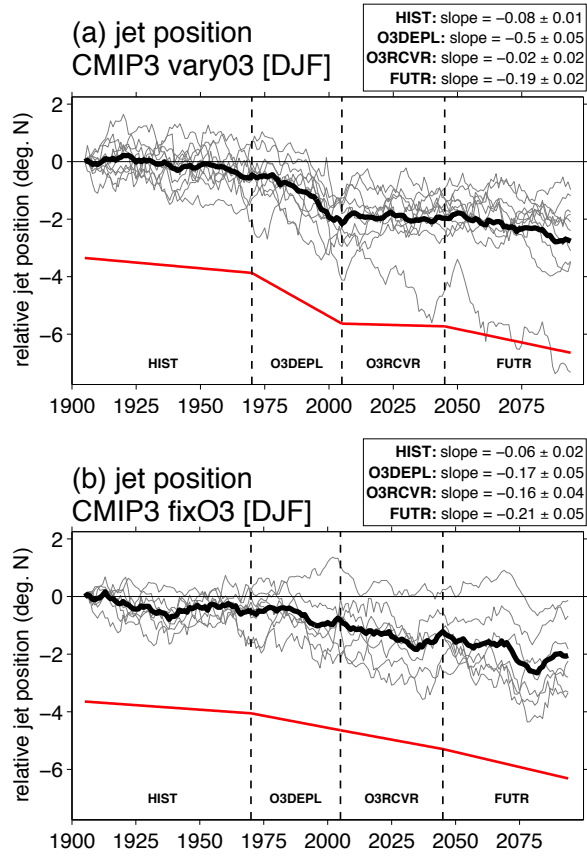


FIG. 4. As in Fig. 1 but for the CMIP3 models, separated by those models (a) with time-varying stratospheric ozone and those (b) with fixed ozone.

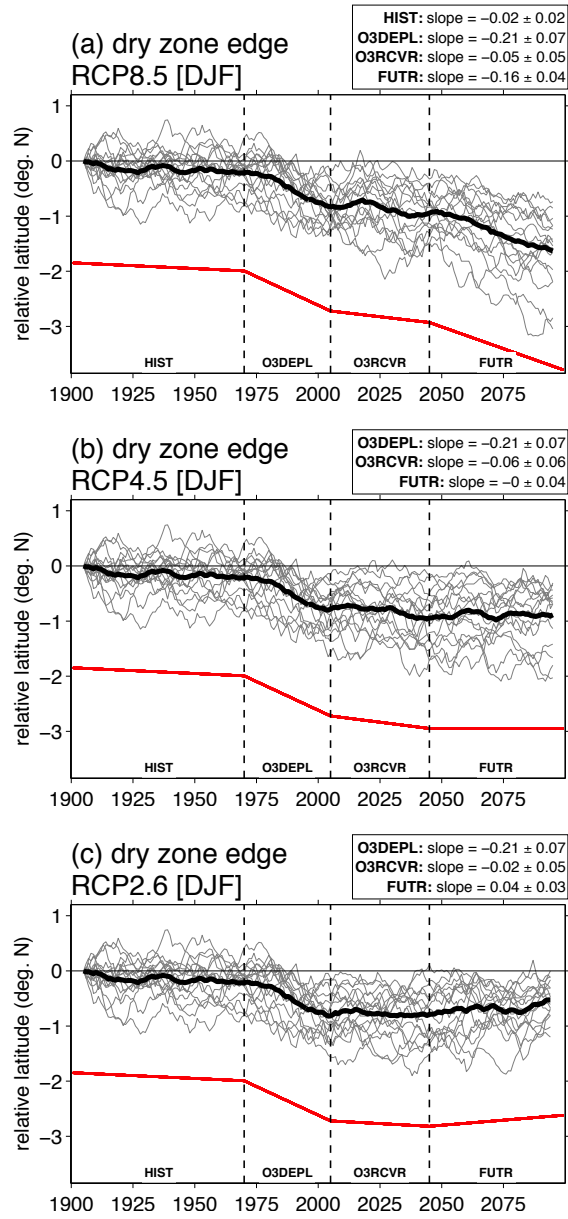


FIG. 5. As in Fig. 1 but for the latitude of the subtropical dry zone edge (precipitation minus evaporation zero-crossing).

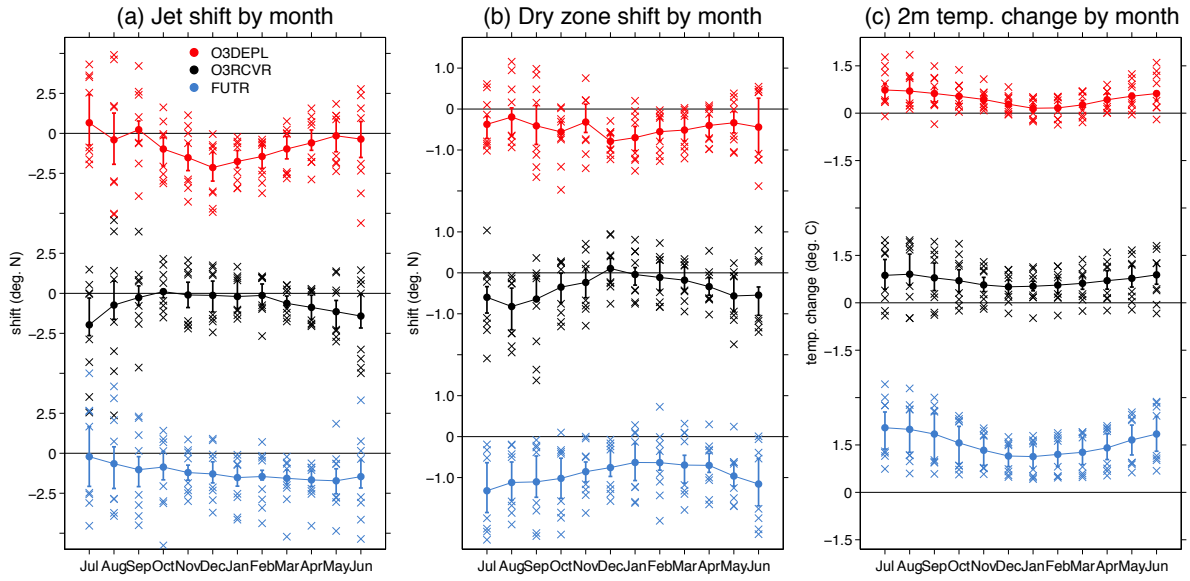


FIG. 6. (a,b) Shift in the Southern Hemisphere (a) jet and (b) dry zone edge (zero-crossing of precipitation minus evaporation) as a function of month for three time periods over the Historical and RCP8.5 scenarios. (c) Similar to (a,b) but for the area-averaged high-latitude (46° - 90° S) two-meter air temperature. In all panels, the bars denote the 25th-75th percentile range and the crosses denote values outside of this interval. The calculation is done as a time-slice difference, and the years used for each time period are given in Table 3.

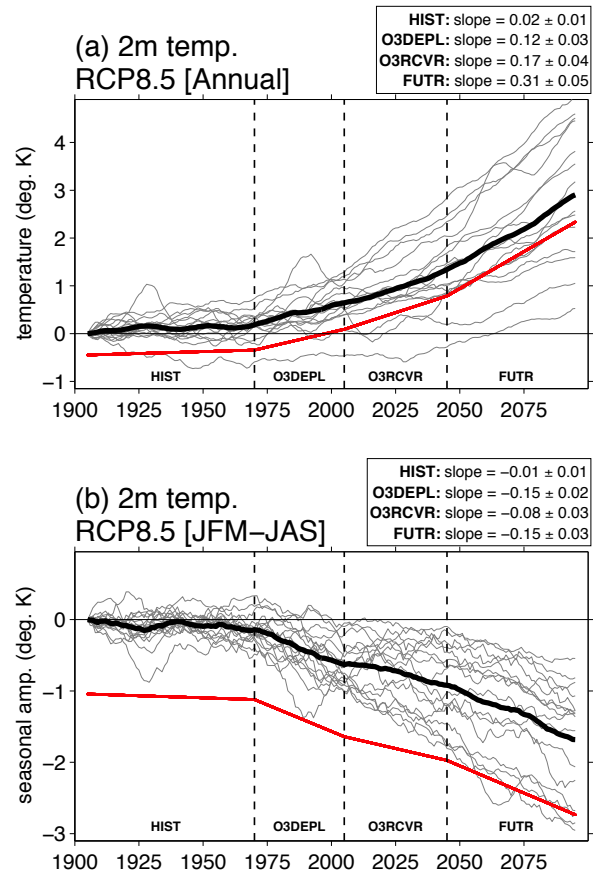


FIG. 7. As in Fig. 1 but for the RCP8.5 high-latitude (46° - 90° S) 2-meter air temperature for (a) the annual-mean and (b) the seasonal amplitude defined as JFM-JAS (summer minus winter).

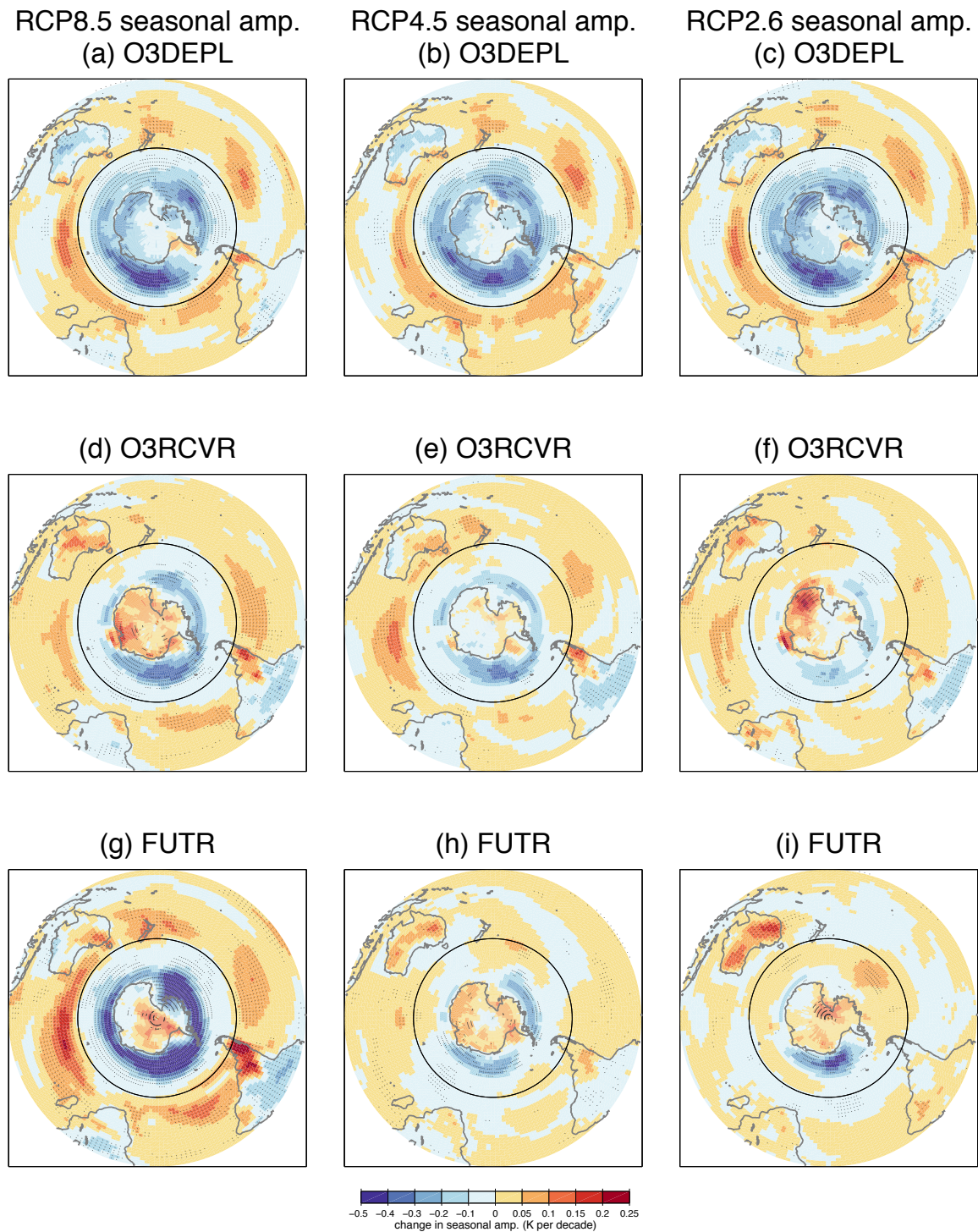


FIG. 8. Multi-model mean change in degrees per decade of the seasonal amplitude of 2-meter air temperatures. Stippling denotes locations where at least 80% of the models (13 of 16) agree on the sign of the change. Solid black lines denote the multi-model mean jet position at the beginning of the O3DEPL period (46° S; see Table 3 for the years included in each period). Fields were interpolated to a 2° by 2° latitude-longitude grid before plotting.

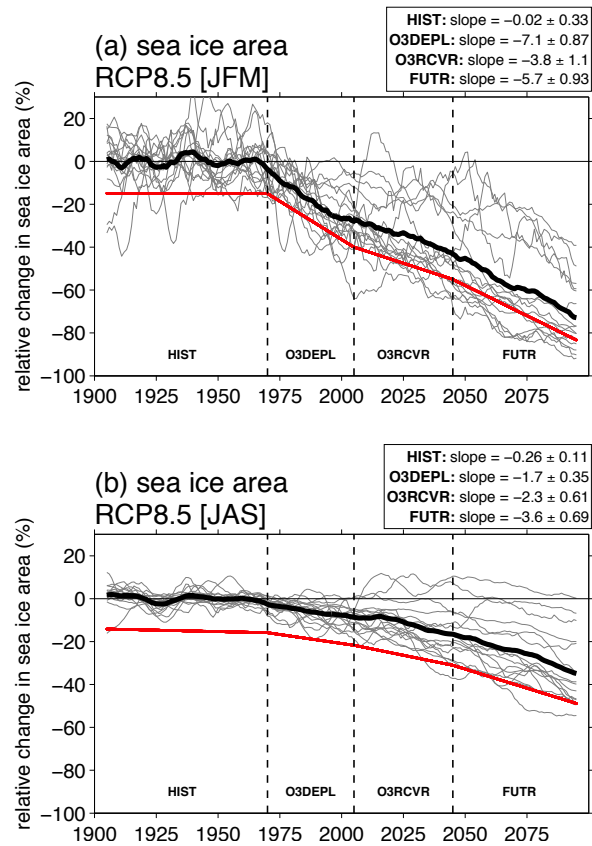


FIG. 9. As in Fig. 1 but for the RCP8.5 JFM and JAS percent change in sea ice area.